nature chemistry

PERSPECTIVE

PUBLISHED ONLINE: 22 NOVEMBER 2016 | DOI: 10.1038/NCHEM.2651

Oriented electric fields as future smart reagents in chemistry

Sason Shaik*, Debasish Mandal and Rajeev Ramanan

Oriented external electric fields (OEEFs) as 'smart reagents' are no longer a theoretical dream. Here, we discuss the wide-ranging potential of using OEEFs to catalyse and control a variety of non-redox reactions and impart selectivity at will. An OEEF along the direction of electron reorganization (the so-called reaction axis) will catalyse nonpolar reactions by orders of magnitude, control regioselectivity and induce spin-state selectivity. Simply flipping the direction of the OEEF or orienting it off of the reaction axis, will control at will the *endo/exo* ratio in Diels–Alder reactions and steps in enzymatic cycles. This Perspective highlights these outcomes using theoretical results for hydrogen abstraction reactions, epoxidation of double bonds, C–C bond forming reactions, proton transfers and the cycle of the enzyme cytochrome P450, as well as recent experimental data. We postulate that, as experimental techniques mature, chemical syntheses may become an exercise in zapping oriented molecules with OEEFs.

This is a Perspective on the prospects of utilizing oriented external electric fields (OEEFs) as future smart catalysts in chemical synthesis. The recent elegant experiment of an OEEF-catalysed Diels–Alder reaction[1] confirmed a previous theoretical prediction[2], and thereby showed that such goals of catalysing non-polar and non-redox reactions by means of OEEFs[3–5] are reachable, and await exploration via iterative improvement of already accessible techniques[1,6–8]. As we shall argue, OEEFs along the reaction axis (where electronic reorganization transpires) awaken the weak ionicity of those covalent bonds that undergo breaking and reformation[9], thereby imparting special stability on transition states of nonpolar reactions.

External electric fields (EEFs) have a range of effects. EEFs affect the spectroscopy of molecules (for example, the Stark Effect)[10,11], promote electron transfer and redox reactions[12–16], and elicit spin-polarized conductivity[17,18]. Intense fields (lasers) change geometries of molecules[19], whereas EEF pulses at STM tips cause isomerization of molecules[20,21] and induce spin-crossover transitions in Fe(II) complexes, thereby serving as single molecular switches[22].

Our interest in catalysis by OEEFs was seeded during Yeshayahu Pocker's 1974 course on electrostatic catalysis of bond heterolysis reactions in concentrated $LiClO_4$ solutions (6–7 M)[23]. Subsequently, it was reawakened during the development of the valence bond (VB)-diagram model of chemical reactivity; this model projects the essential impact of ionic VB structures on chemical reactivity[9,24]. In 1999 we addressed electrostatic catalysis of S_N1 heterolysis by showing how external ions lower the energy of ionic structures and thereby induce rate enhancement[9,25,26]. However, the impulse to start a systematic exploration of OEEF effects on nonpolar reactions was provided by the computed oriented EFs in P450 enzymes, and the effect of single-site mutations on the reorientation of these EFs[27,28]. Based on these studies[2–5], this Perspective tries to chart the horizons of OEEF effects on chemical reactivity of nonpolar reactions, such as H-abstraction, radical addition to double bonds, cycloadditions and so on. Additionally, we demonstrate that the OEEF is an effector of chemical change, acting by selection rules. It alters the kinetics and thermodynamics of the reactions and thereby acts as a catalyst or inhibitor of reactions at will, and as a controller of reaction mechanisms.

Although this Perspective focuses on OEEFs, it is important to mention that nature has already devised chemical objects with built-in electric fields (EFs) that catalyse a variety of reactions by stabilizing ionic structures in their respective transition states. The catalytic power of enzymes has been attributed[29,30] to pre-organized polar groups that stabilize transition states and impart electrostatic catalysis on their respective reactions. Electrostatic catalysis in enzymes was recently demonstrated for ketosteroide isomerase in an experiment[31] that related the stabilization of the transition state for carbonyl-activation directly to the local field of the polar groups[32]. Furthermore, built-in molecular EFs generated by charged substituents were recently found to change bond dissociation energies of remote bonds by tens of kilojoules due to electrostatic stabilization of the generated distonic radicals[33,34]. Ultimately, the application of OEEFs to synthesis may mimic nature and perhaps surpass its designs.

Waking dormant ionic structures by OEEFs

OEEFs wake up dormant ionic structures of bonds and cause dipole orientation in the molecules frame[35–39]. This effect is apparent from Fig. 1a for the homonuclear bonds H–H and Li–Li in a *z*-oriented field along the bond axis. It is seen that a *z*-OEEF induces significant ionicity in these homonuclear bonds. The degree depends on the molecular polarizability (compare H_2 to Li_2) and the field's strength. As seen by comparing the charges in red to those in blue, flipping the field from positive ($F_z > 0$) to negative ($F_z < 0$) flips also the direction of bond ionicity. Increasing the field's strength increases the ionicity (see Supplementary Table 4). For example, doubling F_z to 0.04 a.u. (2.06 V Å^{-1}) increases the charge polarization to ±0.22 e$^-$ for H_2. These changes are specific and they occur only when the OEEF is projected along the bond axis.

Understanding this effect with either molecular orbital (MO) or VB theory is straightforward. Thus, as shown in Fig. 1b, in a zero field the electron pair of the Li–Li bond resides in a symmetric σ MO. In the presence of F_z the direct product of the σ and $\sigma^\star$ orbitals has the same symmetry as the $\boldsymbol{F}_z$ operator. Hence, the orbitals mix and rehybridize, acquiring higher contributions on either the right or left atoms, depending on the direction of F_z.

Institute of Chemistry and The Lise Meitner-Minerva Center for Computational Quantum Chemistry, Hebrew University of Jerusalem, 91904 Jerusalem, Israel.*e-mail: sason@yfaat.ch.huji.ac.il

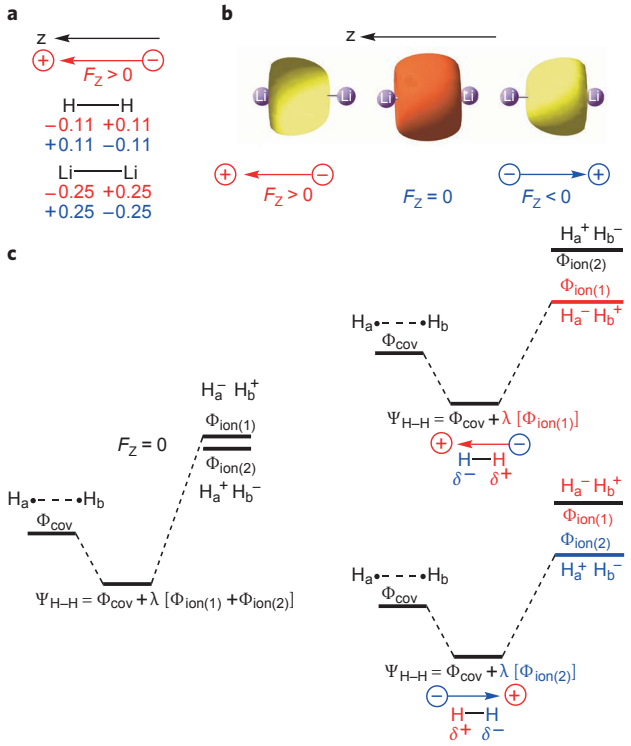

Figure 1 | MO and VB analyses of the manner by which an OEEF, oriented along the bond axis, generates charge distributions and dipole moments in two homonuclear bonds, H–H and Li–Li. a, OEEF-induced ionicity in H_2 and Li_2 for positive ($F_z > 0$) and negative ($F_z < 0$) fields (±0.02 a.u.; 1 a.u. = 51.4 V Å^{-1}) along the bond-axis. **b**, The MO-based polarization mechanism due to σ–σ^* mixing: the symmetric σ orbital of Li_2 without a field (centre) versus the polarized ones for $F_z > 0$ and $F_z < 0$ (on both sides). **c**, The VB-based polarization mechanism: the bond-wave-function (Ψ_{H-H}) without a field (left) arises due to equal mixing of the covalent structure (Φ_{cov}) with the degenerate ionic structures ($\Phi_{ion(1)}$, $\Phi_{ion(2)}$), producing a non-polarized covalent bond. $F_z < 0$ and $F_z > 0$ (right) exert selective stabilization of the ionic structure that opposes the field's polarity. The selective covalent–ionic mixing thereby leads to polarized bond wavefunctions.

Figure 1c shows the VB scenario using the H–H bond. Thus, in a zero field, the H–H electron-pair bond possesses a covalent structure (Φ_{COV}) that mixes equally with two degenerate ionic structures, $\Phi_{ion(1)}$ and $\Phi_{ion(2)}$. Consequently, the bond-wave function (Ψ_{H-H}) describes an apolar bond, even though the ionic structures are hidden dormant in the wave function. However, a z-OEEF stabilizes the ionic structure $\Phi_{ion(1)}$ that now mixes preferentially with the covalent structure and leads to a bond with ionicity oriented as in $\Phi_{ion(1)}$. Flipping the z-OEEF, will now stabilize the ionic structure $\Phi_{ion(2)}$, which will mix preferentially with the covalent structure and lead to a bond with the ionicity of $\Phi_{ion(2)}$.

It is clear that as we increase the field's strength, eventually the specifically stabilized ionic structure will cross below the covalent structure leading to bond heterolysis[25,26], as found indeed recently using detailed computations[39]. All of these effects on the dormant ionic structures will appear at weaker fields for polar bonds, for example ^{t}Bu–Cl, where at $F_z = 0.04$ a.u. the charge distribution is already $^t Bu^{+0.425}Cl^{-0.425}$ (Supplementary Table 6). Thus, the OEEF will catalyse the bond heterolysis, much like the $LiClO_4$ catalysis[23] of S_N1 reactions of polar bonds[25,26,30]. The control of the energetics of ionic structures is the root cause of all the OEEF effects discussed below.

OEEF will drive selective bond activation at will

Let us discuss bond-activation reactions as those promoted by the active species of the enzyme cytochrome P450, called Compound I (**CpdI**). **CpdI** is a high-valent iron-oxo species coupled to a porphyrin (Por) radical cation, thus possessing two closely lying spin states, doublet and quartet, arising from the coupling of the local triplet FeO and the Por radical[27,40,41]. **CpdI** is a versatile reagent that performs C–H hydroxylation, C=C epoxidation, arene activation, oxo-transfers to heteroatoms, and so on[41].

Figures 2 and 3 illustrate the effect of OEEFs on the regioselectivity of epoxidation versus hydroxylation in the reaction of a model **CpdI** with propene.[3] Fig. 2a depicts the coordinate axes and the convention used for positive F_z and dipole (μ_z) oriented along the S–Fe–O axis. Figure 2b displays spin densities and μ_z values in the quartet state (similar trends pertain to the doublet state) in a zero field (in black) and under the influence of F_z (in red and blue). It is seen that in $F_z = 0$, the iron-oxo moiety has two unpaired spins distributed almost equally between Fe and O (1.04 and 0.98, respectively), and a third spin distributed almost evenly over the Por and thiolate (S) ligands. For $F_z < 0$ (in blue) there occurs charge transfer (CT) from Por to S that redistributes the spin density, increasing the Por radical cation character (Por$^{•+}$) at the expense of the thiolate. By contrast, in $F_z > 0$ (in red) an opposite CT transpires and **CpdI** acquires a large S-radical character at the expense of Por$^{•+}$. The z-OEEF also induces significant changes in the dipole-moment components along the z-axis. Thus, in accord with the CT direction, $F_z > 0$ increases the negative value of μ_z from −0.52 D (at $F_z = 0$) to −6.30 D, whereas $F_z < 0$ flips the direction of μ_z and increases its value to 5.27 D. The OEEF augmentation of the dipoles with regard to $F_z = 0$ reflects augmented ionicity of the bonds along the S–Fe–O axis. Let us see if these changes will have any impact on the regioselectivity of bond activation by **CpdI**.

Figures 3a and 3b show the impact of OEEFs on the regioselectivity of bond activation, using the transition states in the rate-determining steps for the two processes; (H-abstraction (**TS1**$_H$) in hydroxylation and an Fe=O attack on the double bond (**TS1**$_C$) in epoxidation)[3]. Fig. 3a plots the spin-states' averaged energy differences between these transition states, as a function of the x,y,z-OEEFs. It is seen that at $F_z = 0$ there is no selectivity, and indeed, Fig. 3b shows that these transition states (for the two spin states) are condensed to within 0.5 kcal mol^{-1}. However, Fig. 3a shows that turning F_z on imparts regioselectivity such that $F_z < 0$ prefers epoxidation, whereas $F_z > 0$ prefers hydroxylation.

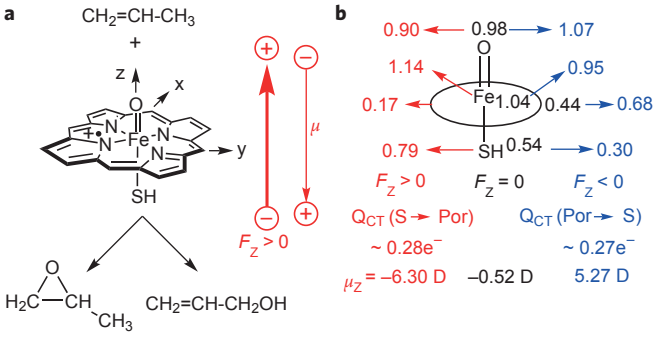

Figure 2 | A z-oriented OEEF affects the bond activation reactions of propene, mediated by an iron-oxo Por radical cation model species (CpdI) of the enzyme cytochrome P450. a, Potential propene activation reactions by **CpdI** to an epoxide and/or an allyl alcohol. The coordinate axes are shown on **CpdI**, along with the used conventions for positive F_z and dipole moment (μ_z). **b**, Spin densities on O, Fe, Por and SH: in the middle in black for $F_z = 0$, whereas to the right (blue) for $F_z < 0$ and to the left (red) for $F_z > 0$. Underneath the structures we indicate amounts and directions of charge transfer (Q_{CT}), and dipole moments (in Debye units) of **CpdI**. Note that the OEEFs in the z-axis increase the dipole moment of **CpdI** in an absolute magnitude, and change its spin density distribution. Figure adapted with permission from ref. 3, ACS.

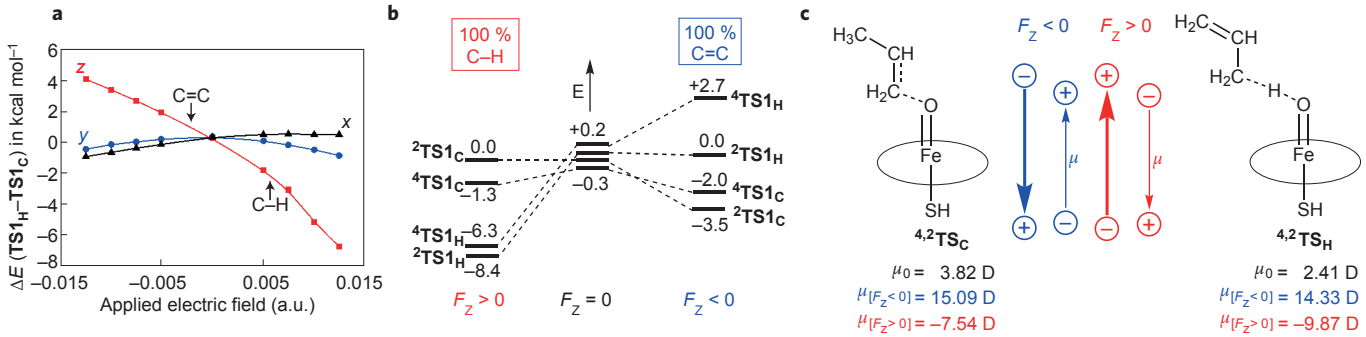

Figure 3 | A *z*-oriented OEEF causes selective bond activations of propene by Cpd I, such that either C–H hydroxylation or C=C epoxidation can be produced at will. a, Plots of the spin-averaged transition-state energy differences ($E(\mathbf{TS_H})$–$E(\mathbf{TS_C})$) for hydroxylation versus epoxidation, as a function of the field strengths and directions along the three axes. Note that a negative F_z favours C=C epoxidation, whereas a positive one favours C–H hydroxylation. OEEFs along the *x*- and *y*-axes are however, ineffective. **b**, Relative energies of the four transition states at $F_z = 0$ and $F_z = \pm 0.0125$ a.u. Without the field there is no selectivity. Turning on the field leads to 100% C–H activation when $F_z > 0$, whereas flipping the field to $F_z < 0$ leads to 100% C=C activation. **c**, The dipole moments for $\mathbf{TS_H}$ and $\mathbf{TS_C}$ increase in absolute magnitudes in positive and negative F_z directions. Note that for $F_z < 0$ $\mathbf{TS_C}$ possesses a larger dipole and will therefore be preferentially stabilized over $\mathbf{TS_H}$, whereas for $F_z > 0$ $\mathbf{TS_H}$ develops a larger dipole and it will be preferentially stabilized over $\mathbf{TS_C}$. Figure adapted with permission from ref. 3, ACS.

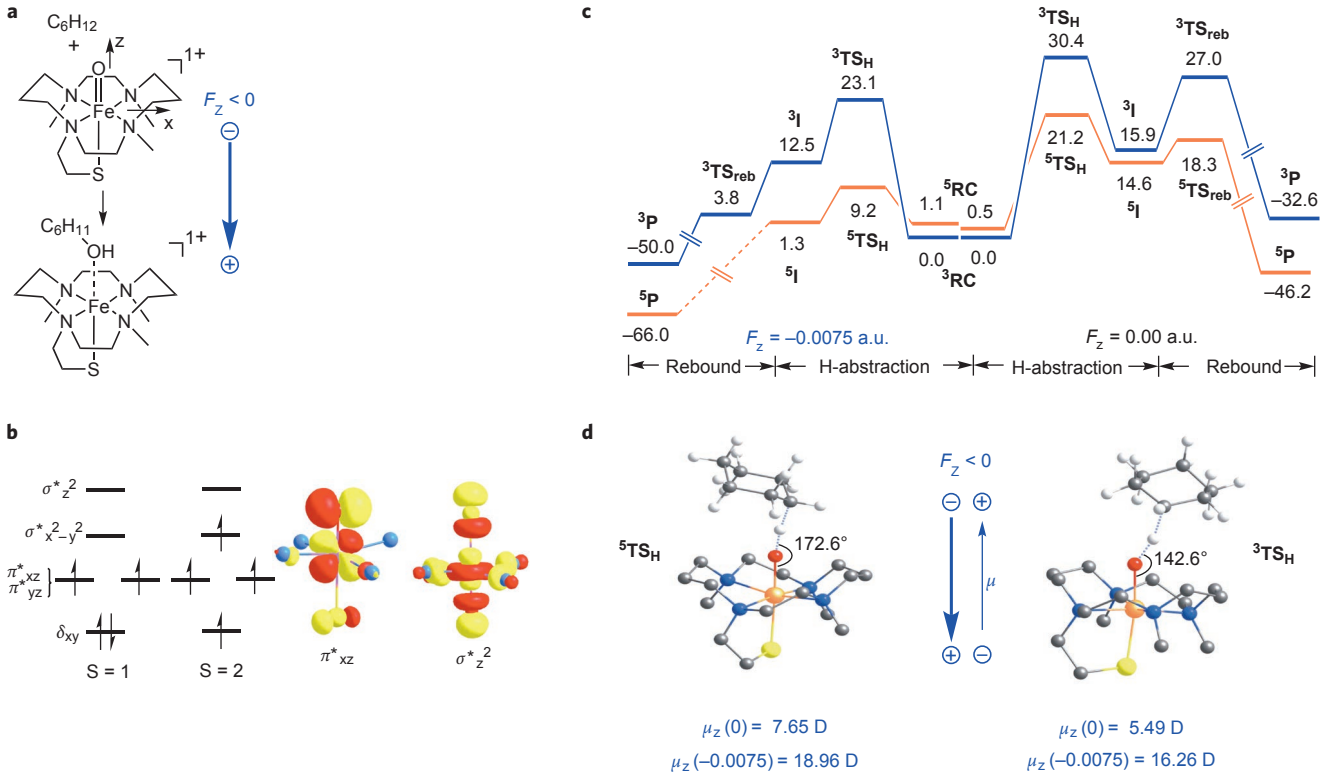

Figure 4 | A negatively oriented *z*-OEEF drastically lowers the C–H hydroxylation barriers in the reactions between the two spin states of an iron-oxo complex (TMC(SR)FeO$^+$) and cyclohexane, and creates product- and spin-state selectivities in the quintet state's hydroxylation process. a, The putative reaction between TMC(SR)FeO$^+$ and C_6H_{12} shown along with coordinate axes (TMC(SR) is a tetramethylcylam with a tethered thiolate). **b**, The *d*-type orbitals and their occupancies in the S=1 (triplet) and S=2 (quintet) spin-states. The depicted $\sigma^*_{z^2}$ and π^*_{xz} orbitals control the geometries of the H-abstraction transition states ($^{5,3}\mathbf{TS_H}$) in the two spin states (the superscripts, for example, in $^3\mathbf{TS_H}$, indicate spin multiplicities). **c**, Zero-point energy and solvent corrected energy (kcal mol^{-1}) profiles with H-abstraction and rebound phases; for $F_z = 0$ to the right and $F_z = -0.0075$ a.u. to the left. Note that when the field is turned on, the barriers decrease, and more so for the quintet state. **d**, Geometries of $^{5,3}\mathbf{TS_H}$ and dipole moments at $F_z = 0$ and $F_z = -0.0075$ a.u. Note that the larger acquired dipole for the quintet transition state with regard to the triplet state, leads also to spin-state selectivity.

VB modelling of the two reactions[42,43] shows that above the covalent states (structures) there exist excited states involving charge transfer for example, from the propene to **CpdI**, along the *z*-axis, and are therefore highly susceptible to *z*-OEEF effects. Indeed, as shown in Fig. 3c, F_z increases the dipole moments of the respective transition states, due to stabilization of the ionic structures along the *z*-axis. Thus, $F_z < 0$ increases CT from the propene moiety towards **CpdI** such that the transition state dipole stretches now from the positively-charged propene to the negatively-charged thiolate. This dipole increase is more pronounced for $\mathbf{TS_C}$ (in the two spin states). On the other hand, $F_z > 0$ induces CT from the thiolate towards the propene, hence flipping the dipole that stretches now from the

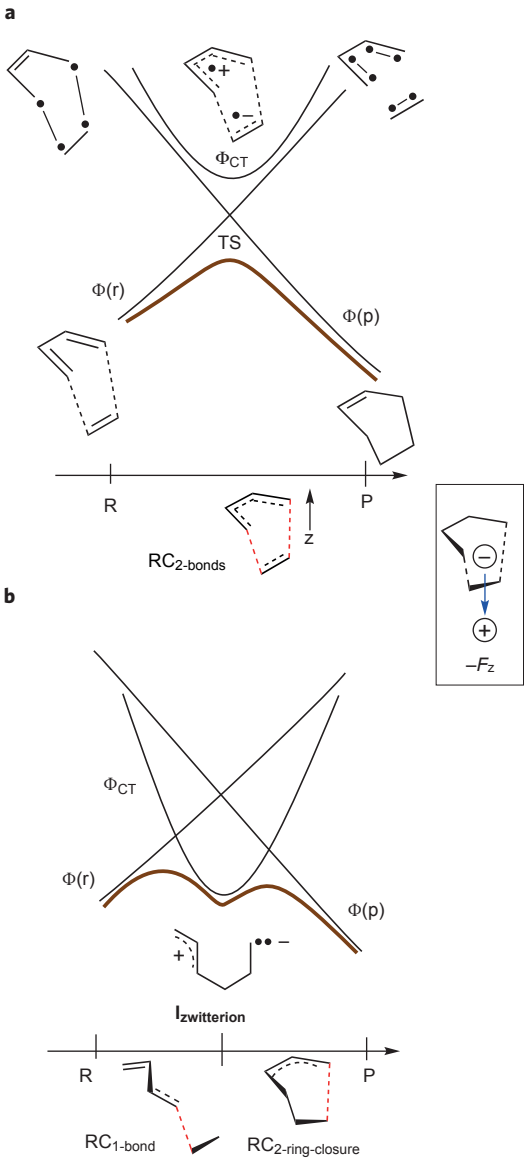

Figure 5 | VB diagrams showing the construction of the energy profiles (brown) for a Diels–Alder reaction between generic diene and dienophile, and leading to predictions of *z*-OEEF effects on catalysis/inhibition and mechanistic crossover in the reactions. a, Formation of the transition state due to the mixing of reactants' and products' state-curves (Φ(r), (Φ(p)) and the CT state (Φ_{CT}), along the concerted pathway. The bold brown curve is the final state's energy profile arising from the VB mixing. $F_z < 0$ will stabilize Φ_{CT} and catalyse the reaction. **b**, The crossing of Φ_{CT}, at some large $F_z < 0$ below the crossing point of the Φ(r) and Φ(p) curves, thus mediating a stepwise mechanism with an intermediate, $\mathbf{I}_{zwitterion}$. Figure adapted with permission from ref. 2, Wiley-VCH.

positively charged thiolate to a negatively charged oxo-ligand. This flipped dipole increases in absolute magnitude compared to the field-free transition states, and the effect is larger for $\mathbf{TS}_H$ ($\mu_z = -9.87$ D versus −7.54 D). Thus, the interaction between F_z and the dipole confers regioselectivity to the reaction, and as seen in Fig. 3b, when the field is sufficiently large, one has regioselectivity at will; 100% hydroxylation at $F_z > 0$ or 100% epoxidation at $F_z < 0$.

The reaction-axis rule. Importantly, in Fig. 3, the *x,y* fields ($F_{x,y}$) induce greater *x,y* dipoles than those produced by F_z (ref. 3). Nevertheless, by contrast to the F_z effects, applying $F_{x,y}$ in Fig. 3a does not impart significant regioselectivity. The reason for this directional selectivity of the electric field is that the dipole changes in the *z*-direction are selectively larger for the transition states with regards to the reactant states, thus leading to catalysis and selectivity. On the other hand, the greater dipoles induced by the $F_{x,y}$ oriented fields do not vary significantly between reactants and transition states and hence they do not impart either catalysis or selectivity. It is apparent that the effect obeys the following selection rule: an EF oriented along the axis wherein the electronic reorganization occurs will catalyse the reaction and endow it with selectivity, it does so by enhancing the stability of the ionic structures that contribute to the transition state and thereby manipulating the barriers. We refer to this as the 'reaction-axis rule'.

OEEF will elicit spin-selective reactions

Non-heme iron-oxo complexes are bio-inspired by the respective ubiquitous natural enzymes, which utilize such complexes to hydroxylate strong C–H bonds. To test the OEEF impact on this biomimetic process, we selected the synthetic TMC(SR)FeO$^+$ complex shown in Fig. 4a (ref. 44), and examined its hydroxylating capability with cyclohexane, which has a strong C–H bond[4]. This specific reaction was chosen, because in the absence of an appropriately oriented OEEF, TMC(SR)FeO$^+$ cannot really abstract a hydrogen from cyclohexane, let alone undergo full hydroxylation to cyclohexyl alcohol. But will it do so with OEEF? Like similar complexes, TMC(SR)FeO$^+$ also possesses two low-lying spin states, triplet (S=1) and quintet (S=2), which are shown in Fig. 4b using the corresponding *d*-orbital diagrams.

Based on the reaction-axis rule, the H-abstraction reaction will be catalysed by a field oriented in the negative direction of the S–Fe–O axis ($F_z < 0$). Figure 4c shows the energy profiles in acetonitrile solution at zero field to the right, and at $F_z = -0.0075$ a.u. to the left; both involving an H-abstraction step and forming radical-intermediate complexes (^{5,3}**I**) followed by radical-rebounds to form the cyclohexanol ferrous-complex products (^{3,5}**P**). It is seen that at $F_z = 0$, the H-abstraction barriers are high, and the rebound barriers are significant. As such, the H-abstraction will be sluggish, and the so-formed cyclohexyl radical will escape the ^{5,3}**I** complex and will give rise to products nascent from this radical[45]. Turning on the F_z in the negative direction leads to dramatic changes; the H-abstraction barrier gets significantly lowered while the rebound barrier vanishes. The effect is spin-selective and larger for the quintet state. At $F_z = -0.0075$ a.u. the H-abstraction barrier for the quintet state becomes very small (9.2 kcal mol^{-1}) and the rebound barrier vanishes altogether, thereby generating an effectively concerted process leading to the alcohol-complex product (similarly, see Supplementary Fig. 1). Thus, product- and spin-selectivities, and catalysis are achieved by the *z*-OEEF along the reaction axis.

The marked increase of μ_z in $^{5,3}\mathbf{TS}_H$ (Fig. 4d) reflects the augmented contributions of the ionic structures $O^- H^+ R^\bullet$ and $O^- H^\bullet R^+$ (R = cyclohexyl) that are stabilized by $F_z < 0$, and contribute to the transition states. These ionic structures are contributed by the OEEF-enhanced mixing of the CT state that involves transfer of an electron from the alkane to the iron-oxo complex[42,43], into the covalent state of the transition state. The spin selectivity of this effect reflects the different transition state geometries (Fig. 4d), which derive from the orbital-selection rules[46] that control the geometries of the respective transition states; σ_z^{*2} controls $^5\mathbf{TS}_H$, whereas $\pi^*_{xz/yz}$ controls $^3\mathbf{TS}_H$ (Fig. 4a). Thus, $^5\mathbf{TS}_H$ has an upright structure, and hence its ionic structures are precisely aligned along the reaction axis, its μ_z increases markedly, and so does its stabilization by the *z*-OEEF. By contrast, $^3\mathbf{TS}_H$ assumes a sideways orientation, and its ionic structure is off the *z*-axis, thus the increase of its μ_z is smaller and its stabilization is lesser, compared with $^5\mathbf{TS}_H$.

Clearly, once again we can see the reaction-axis rule in action, and now due to spin-selective augmentation of the ionic structures

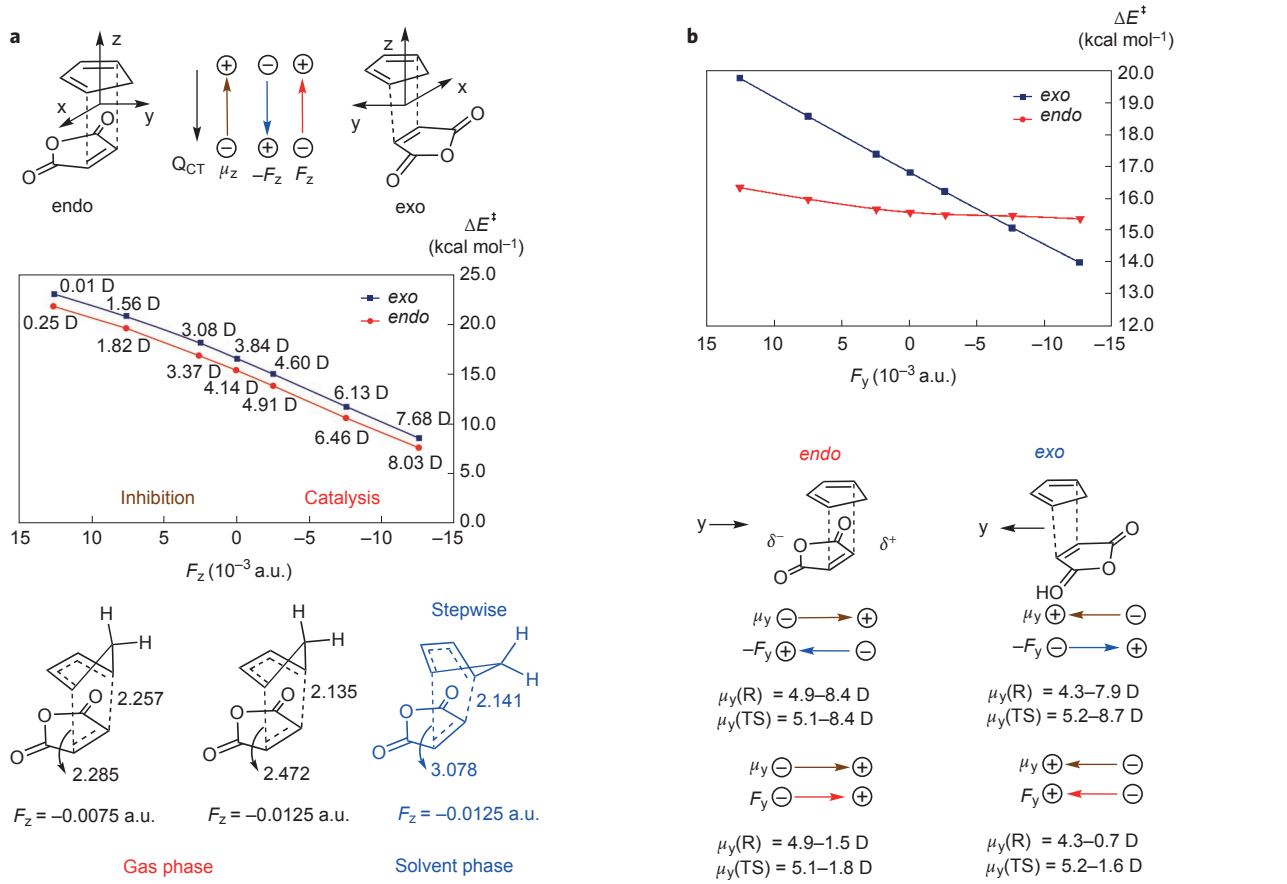

Figure 6 | Computational results showing that OEEFs induce catalysis, inhibition, and *endo/exo* selectivity in the reaction of cyclopentadiene and maleic anhydride. a, F_z induces either catalysis or inhibition depending on the direction: plots of the computed barriers ($\Delta E^{\ddagger}$) for the *endo* and *exo* paths versus F_z. Numbers on the plots are TS-dipole moments (μ_z units are in Debye). The *endo* and *exo* paths (along with the coordinate axes, the applied F_z directions, the direction of transition-state dipole moments and the directions of CT(Q_{CT})) are shown above the barrier plot. Thus, $F_z < 0$ catalyses the reaction, whereas $F_z > 0$ inhibits it. Below the barriers plots are transition-state structures at some $F_z < 0$ values, in the gas phase (structures in black) and in a solvent phase (structure in blue). **b**, F_y induces stereochemical selectivity: $\Delta E^{\ddagger}_{exo/endo}$ plots versus F_y. The *endo* and *exo* paths are shown underneath the barrier plot (along with the directions of the *y*-axis, and the μ_y components in the reactant clusters (**R**) and the corresponding transition states, for $F_y < 0$ and $F_y > 0$). F_y is seen to induce selectivity at will. Figure adapted with permission from ref. 2, Wiley-VCH.

in the transition state[9,24,25]; thus leading to catalysis and product selectivity, and conferring spin-selectivity on the reaction.

Catalysis of Diels–Alder reactions by OEEFs

The Diels–Alder reaction involves simultaneous creation of two C–C bonds, and is therefore a key reaction in organic synthesis. Let us then utilize the reaction-axis rule and make initial predictions about OEEF effects on the reaction. Subsequently we shall compare these predictions to the computational results[2] and the experimental verification of the predictions[1].

Figure 5a shows the VB diagram[2,24,25] that describes the formation of the transition state, the respective barrier, and the mechanistic crossover, for a generic Diels–Alder reaction. Thus, the barrier and transition state arise from the mixing of the reactants' and products' (Φ(r) and Φ(p)) state-curves that cross one another along the concerted pathway. There is also CT-state-curve (Φ_{CT}), which involves an electron transfer from the diene to the dienophile. Φ_{CT} shares the same symmetry as the transition state and can mix into it[25], thus lowering the barrier and endowing the transition state with some ionicity. It is clear that $F_z < 0$ along the reaction axis will stabilize Φ_{CT}, and will cause greater transition state stabilization and hence also catalysis of the reaction. By contrast, $F_z > 0$ will destabilize the Φ_{CT} state, hence decreasing its mixing into the transition state and raising the barrier, thus inhibiting the reaction. Furthermore, as shown in Fig. 5b, at some critically large $F_z < 0$ the Φ_{CT} state should be sufficiently stabilized to cross well below the principal state-curves and change thereby the mechanism from a concerted to a stepwise cycloaddition via a zwitterionic intermediate ($\mathbf{I_{zwitterion}}$).

The calculations support these predictions. Figure 6a shows the variation of the barriers for the *endo* and *exo* cycloadditions of maleic anhydride and cyclopentadiene as a function of the *z*-OEEF. It is seen that $F_z < 0$ lowers the barrier by up to ~8 kcal mol^{-1}, which amounts to million-fold rate-enhancement. By contrast, applying $F_z > 0$ increases the barrier by 6.4 kcal mol^{-1}, thus inhibiting the reaction. The numbers adjacent to the data points on the barrier-plots in Fig. 6a indicate the μ_z dipole-moment components of the transition states. It is seen that $F_z < 0$ increases the dipole moment, whereas $F_z > 0$ decreases it to almost zero. These dipole variations are proportional to the amount of charge transfer (Q_{CT}), from cyclopentadiene to maleic anhydride, induced by stabilization/destabilization of Φ_{CT} and its OEEF modulated-mixing into the transition state's wave function. In accord with the above VB predictions, the calculated Q_{CT}(**TS**) values increase from 0.33 e$^-$ at $F_z = 0$ to 0.55 e$^-$ at $F_z < 0$, while decreasing to 0.16 e$^-$ at $F_z > 0$. This variation of transition state bond ionicity manipulates the barrier heights.

As further seen at the bottom of Fig. 6a, the OEEF affects also the transition state's geometries, which become asynchronous. In the gas-phase the asynchronicity in the two C–C bond making steps

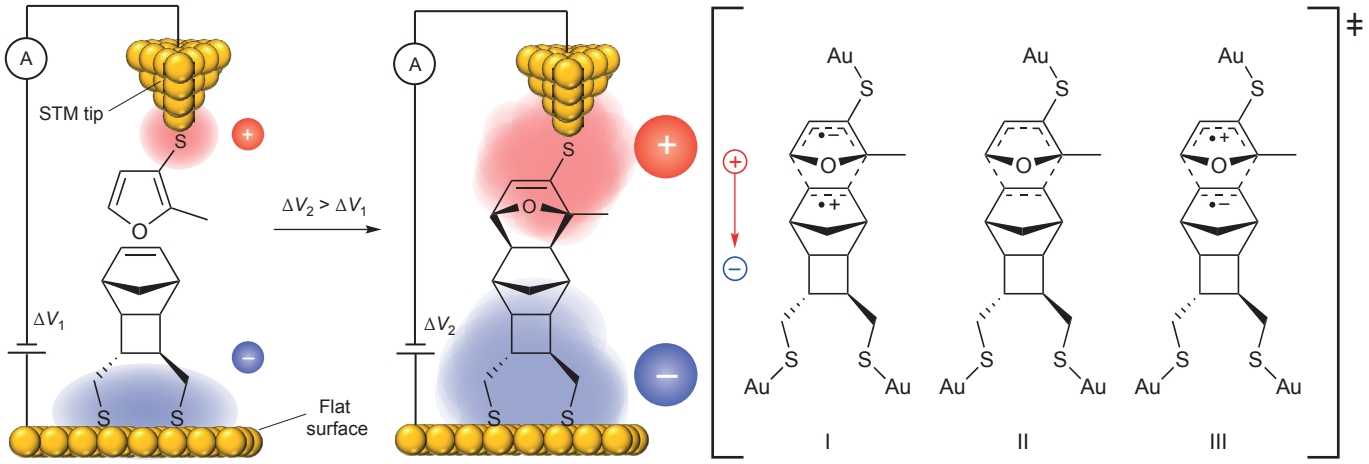

Figure 7 | The single-molecule experiment[1] showing catalysis of a Diels–Alder reaction by an OEEF, created by a bias voltage between the STM tip and the electrode. It is seen from the right-hand drawing that only one direction of the OEEF, the one stabilizing VB structure (I) leads to catalysis. Figure adapted with permission from ref. 1, Nature Publishing Group.

reaches 0.337 Å at the highest negative field, while the mechanism is still being concerted. When solvent (CH_2Cl_2) is added, the asynchronicity reaches 0.887 Å at $F_z = -0.0075$ a.u., but nonetheless the reaction maintains its concerted mechanism. However, it becomes stepwise at a larger negative field, $F_z = -0.0125$ a.u. (with solvent included), proceeding via an open-zwitterionic intermediate, as predicted by the VB model in Fig. 5b (ref. 2).

Finally, Fig. 6b shows another OEEF effect, now along the *y*-axis wherein the maleic anhydride has a dipole moment. It is observed that using $F_y < 0$, the barrier for the *exo*-reaction is lower than for *endo*, whereas when $F_y = 0$ and $F_y > 0$, the preferred stereochemistry is *endo*. Again, as seen from the dipole moments underneath the barriers plots, the selectivity crossover is rooted in transition state bond-ionicity changes. $F_y < 0$ increases the *y*-dipole component for $\mathbf{TS}_{exo}$ compared with the respective reactant cluster (**R**). This increase is less effective for $\mathbf{TS}_{endo}$, thus leading to *exo* selectivity. On the other hand, for $F_y > 0$ the native dipoles are parallel to the field's polarity and hence, both **R** and **TS** are destabilized. In the *endo*-path both species have similar dipoles and undergo equal destabilization, thus the *endo* barrier remains constant as F_y changes. In comparison, $\mathbf{TS}_{exo}$ having the higher dipole undergoes larger destabilization with regard to $\mathbf{R}_{exo}$, and hence the exo-barrier rises for $F_y > 0$. Secondary-orbital interactions may play some role but certainly not in the *endo*/*exo* selectivity crossover.

In summary therefore, usage of OEEFs enables to control catalysis/inhibition of the Diels–Alder reaction and its *endo*/*exo* selectivity at will.

Experimental verification. The OEEF catalysis of a Diels–Alder reaction was experimentally verified by Aragonès *et al.*[1] using the set-up shown schematically in Fig. 7. Thus, the authors of this study ingeniously solved the orientations of the reactants and EEF along the reaction axis, using an STM tip holding the diene and a self-assembled dienophile on a gold electrode. The OEEF was created by a voltage difference between the tip and the electrode. By moving the tip towards the electrode, up to ~1 nm, the team observed a tunnelling current, which marked the formation of a product molecule that generated a conduction junction. They convincingly ascertained that only the product leads to the tunnelling current. The frequency of product formation event was studied using the break-junction (BJ) technique[21], which provides a statistically meaningful reaction rate. The team was able to verify that catalysis of the reaction occurred at the specific field orientation that stabilized only the CT state with the lower energy (marked (I) in Fig. 7). This refined single-molecule experiment is a proof of principle that nonpolar reactions involving C–C bond formation are subject to OEEF catalysis. It further shows the way to orient the reacting molecules and fix them within the field.

Prospects and conclusions

In summary, use of OEEFs along the reaction-axis enables chemists to control catalysis/inhibition of nonpolar reactions and their selectivity patterns at will by enhancing or retarding the electronic reorganization required to convert reactants to products. The effects are mediated via ionic structures whose variability manipulates barrier heights[9,25].

The number of potential applications is vast. Recently[5] we showed that an OEEF, along the S–Fe axis, could control the entire catalytic cycle of P450, by either inhibiting or catalysing any step in the cycle by merely flipping the field's polarity in the direction of the reaction axis or bond axis. This includes gating of the cycle by a water-ligand detachment, electron-transfer steps, O_2 uptake and protonation of the Fe–O_2 moiety. Polar bonds[35,37] behave intriguingly under OEEFs; for example, C–Cl (Supplementary Table 6) undergoes enhanced ionicity in one OEEF direction, and in the reverse the OEEF quenches and flips bond-polarity. Other unpublished data show that the Menshutkin reaction and DNA lesions are prone to catalysis by OEEF, and so is an entirely nonpolar class of radical exchange reactions, $R^{\bullet} + H\text{–}R' \rightarrow R\text{–}H + R'^{\bullet}$, for example. Coote *et al.* reported analogous experimental[34] and theoretical results[33] on H-abstraction, using built in EFs due to remote charged substituents. Other theoretical and experimental studies reported OEEF catalysis of proton transfer[8,47–50] and tautomerization[11,51] reactions, biological regulation of NO release[52], control of metal-ligand binding[36,37,53], formation of amino acids from simple molecules (the Miller experiment testing the postulate of prebiotic generation of amino acids by electric discharge)[54], and affect guanine aggregates[55]. These are just a few of the applications in the huge landscape of OEEF-controlled reactivity, showing that OEEF is a mighty effector of chemical change.

The theoretical predictions still face some fundamental challenges, which await treatment. One of these is the question of the favoured orientation of the EEF. Thus, it is already clear that while the reaction axis forms a reliable selection rule for catalysis and inhibition, some selectivity effects (for example, *exo* and *endo* in Diels–Alder reactions) requires OEEF orientation off of the reaction axis. In some cases the reaction axis may not be well defined. Deriving the selection rule for a symmetry forbidden reaction[56] is a challenge, for which we have already made progress. Proper treatment of solvent effect in the presence of OEEF will require molecular dynamics simulation along with the quantum mechanical calculations.

Although not every EEF effect requires orientation[57], most effects do, such that orientation poses an experimental challenge. As noted above (Fig. 7), the STM-BJ technique provides an elegant solution for the orientational problem of the reactants and the EEF, thus nimbly controlling reactivity of single molecules[1]. Kanan and co-workers[6,7] introduced an electrochemical cell that provides interfacial EEFs that control the selectivity of rearrangement and carbene reactions. As envisioned by Kanan, his technique can be eventually exploited on a preparative scale. There exists also a micro reactor[8] that enables the study of gas- and solution-phase reactions under EEF. Nevertheless, orienting the field in particular directions, and/or fixing the reactant molecules within the field, remains a challenge for preparative applications. Some progress should come by use of cells with self-assembled-reactants[58] (as demonstrated recently by Ciampi and co-workers) for the study of redox activity of tethered radicals on modified Si(100) electrodes[59]. Once the orientational problem (reactants versus EEF) is overcome and allows reactions on a preparative scale, one can envision chemical synthesis being powered up by OEEFs. OEEFs have the potential of becoming the smart reagents and effectors of chemical changes of the future.

Received 14 June 2016; accepted 20 September 2016; published online 22 November 2016

References

1. Aragonés, C. *et al.* Electrostatic catalysis of a Diels–Alder reaction. *Nature* **531,** 88–91 (2016).
2. Meir, R., Chen, H., Lai, W. & Shaik, S. Oriented electric fields accelerate Diels–Alder reactions and control the endo/exo selectivity. *ChemPhysChem* **11,** 301–310 (2010).
3. Shaik, S., de Visser, S. P. & Kumar, D. External electric field will control the selectivity of enzymatic-like bond activations. *J. Am. Chem. Soc.* **126,** 11746–11749 (2004).
4. Hirao, H., Chen, H., Carvajal, M. A., Wang, Y. & Shaik, S. Effect of external electric fields on the C–H Bond activation reactivity of nonheme iron–oxo reagents. *J. Am. Chem. Soc.* **130,** 3319–3327 (2008).
5. Lai, W., Chen, H., Cho, K.-B. & Shaik, S. External electric field can control the catalytic cycle of cytochrome P450cam: a QM/MM Study. *J. Phys. Chem. Lett.* **1,** 2082–2087 (2010).
6. Gorin, C. F., Beh, E. S. & Kanan, M. W. An electric field-induced change in the selectivity of a metal oxide-catalyzed epoxide rearrangement. *J. Am. Chem. Soc.* **134,** 186–189 (2012).
7. Gorin, C. F., Beh, E. S., Bui, Q. M., Dick, G. R. & Kanan, M. W. Interfacial electric field effects on a carbene reaction catalyzed by Rh porphyrins. *J. Am. Chem. Soc.* **135,** 11257–11265 (2013).
8. Susarrey-Arce, A. *et al.* A new ATR-IR microreactor to study electric field-driven processes. *Sensors and Actuators B: Chemical* **220,** 13–21 (2015).
9. Hiberty, P. C., Megret, C., Song, L., Wu, W. & Shaik, S. Barriers for hydrogen *vs.* halogen exchange — an experimental manifestation of charge-shift bonding. *J. Am. Chem. Soc.* **128,** 2836–2843 (2006).
10. Fried, S. D. & Boxer, S. G. Measuring electric fields and noncovalent interactions using the vibrational stark effect. *Acc. Chem. Res.* **48,** 998–1006 (2015).
11. Oklejas, V., Sjostrom, C. & Harris, J. M. SERS detection of the vibrational stark effect from nitrile-terminated SAMs to probe electric fields in the diffuse double-layer. *J. Am. Chem. Soc.* **124,** 2408–2409 (2002).
12. Franzen, S., Goldstein, R. F. & Boxer, S. G. Electric field modulation of electron transfer reaction rates in isotropic systems: long distance charge recombination in photosynthetic reaction centers. *J. Phys. Chem.* **94,** 5135–5149 (1990).
13. Lao, K., Franzen, S., Stanley, R. J., Lambright, D. G. & Boxer, S. G. Effects of applied electric fields on the quantum yields of the initial electron-transfer steps in bacterial photosynthesis. 1. quantum yield failure. *J. Phys. Chem.* **97,** 13165–13171 (1993).
14. Murgida, D. H. & Hildebrandt, P. Electron-transfer processes of cytochrome *c* at interfaces. New insights by surface-enhanced resonance raman spectroscopy. *Acc. Chem. Res.* **37,** 854–861 (2004).
15. Wahadoszamen, M., Nakabayashi, T., Kang, S., Imahori, H. & Ohta, N. External electric field effects on absorption and fluorescence spectra of a fullerene derivative and its mixture with zinc-tetraphenylporphyrin doped in a PMMA film. *J. Phys. Chem. B* **110,** 20354–20361 (2006).
16. Ohta, N., Koizumi, M., Umeuchi, S., Nishimura, Y. & Yamazaki, I. External electric field effects on fluorescence in an electron donor and acceptor system: ethylcarbazole and dimethyl terephthalate in PMMA polymer films. *J. Phys. Chem.* **100,** 16466–16471 (1996).
17. Son, Y. W., Cohen, M. L. & Louie, S. G. Half-metallic graphene nanoribbons. *Nature* **444,** 347–349 (2006).
18. Naaman, R., Waldeck, D. H. Spintronics and chirality: spin selectivity in electron transport through chiral molecules. *Annu. Rev. Phys. Chem.* **66,** 263–281 (2015).
19. Hishikawa, A., Iwamae, A. & Yamanouchi, K. Ultrafast deformation of the geometrical structure of CO_2 induced in intense laser fields. *Phys. Rev. Lett.* **83,** 1127–1130 (1999).
20. Alemani, M. *et al.* Electric field-induced isomerization of azobenzene by STM. *J. Am. Chem. Soc.* **128,** 14446–14447 (2006).
21. Darwish, N., Aragonès, A. C., Darwish, T., Ciampi, S. & Díez-Pérez, I. Multi-responsive photo- and chemo-electrical single-molecule switches. *Nano Lett.* **14,** 7064–7070 (2014).
22. Harzmann, G. D., Frisenda, R., van der Zant, H. S. & Mayor, M. Single-molecule spin switch based on voltage-triggered distortion of the coordination sphere. *Angew. Chem. Int. Ed.* **54,** 13425–13430 (2015).
23. Pocker, Y. & Buchholz, R. F. Electrostatic catalysis by ionic aggregates. II. Reversible elimination of hydrogen chloride from tert-butyl chloride and the rearrangement of 1-phenylallyl chloride in lithium perchlorate-diethyl ether solutions. *J. Am. Chem. Soc.* **92,** 4033–4038 (1970).
24. Shaik, S. S. What happens to molecules as they react? A valence bond approach to reactivity. *J. Am. Chem. Soc.* **103,** 3692–3701 (1981).
25. Shaik, S. & Shurki, A. Valence bond diagrams and chemical reactivity. *Angew. Chem. Int. Ed.* **38,** 586–625 (1999).
26. Pross, A. & Shaik, S. S. A qualitative valence bond approach to organic reactivity. *Acc. Chem. Res.* **16,** 363–370 (1983).
27. Cho, K.-B. *et al.* Compound I in heme thiolate enzymes: a comparative QM/MM study. *J. Phys. Chem. A* **112,** 13128–13138 (2008).
28. Dandamudi, U. et al. A single-site mutation (F429H) converts the enzyme CYP 2B4 to a heme-oxygenase: a QM/MM study. *J. Am. Chem. Soc.* **134,** 4053–4056 (2012).
29. Warshel, A., Sharma, P. K., Kato, M., Xiang, Y., Liu, H. & Olsson, M. H. M. Electrostatic basis for enzyme catalysis. *Chem. Rev.* **106,** 3210–3235 (2006).
30. Warshel, A. Electrostatic basis of structure-function correlation in proteins. *Acc. Chem. Res.* **14,** 284–290 (1981).
31. Fried, S. D., Bagchi, S. & Boxer, S. G. Extreme electric fields power catalysis in the active site of ketosteroid isomerase. *Science* **346,** 1510–1514 (2014).
32. Liu, C. T. *et al.* Probing the electrostatics of active site microenvironments along the catalytic cycle for e*scherichia coli* dihydrofolate reductase. *J. Am. Chem. Soc.* **136,** 10349–10360 (2014).
33. Gryn'ova, G., Marshall, D. L., Blanksby, S. J. & Coote, M. L. Switching radical stability by pH-induced orbital conversion. *Nat. Chem.* **5,** 474–481 (2013).
34. Klinska, M., Smith, L. M., Gryn'ova, G., Banwell, M. G. & Coote, M. L. Experimental demonstration of pH-dependent electrostatic catalysis of radical reactions. *Chem. Sci.* **6,** 5623–5627 (2015).
35. Sowlati-Hashjin, S. & Matta, C. The chemical bond in external electric fields: energies, geometries, and vibrational Stark shifts of diatomic molecules. *J. Chem. Phys.* **139,** 144101 (2013).
36. De Biase, P. M. *et al.* Molecular basis for the electric field modulation of cytochrome *c* structure and function. *J. Am. Chem. Soc.* **131,** 16248–16256 (2009).
37. Karafiloglou, P. Control of delocalization and structural changes by means of an electric field. *J. Comput. Chem.* **27,** 1883–1891 (2006).
38. Wei, Y. *et al.* A theoretical study of the activation of nitromethane under applied electric fields. *RSC Adv.* **6,** 24712–24718 (2016).
39. Schirmer, B. & Grimme, S. Electric field induced activation of H_2 — can DFT do the job? *Chem. Commun.* **46,** 7942–7944 (2010).
40. Shaik, S., Kumar, D., de Visser, S. P., Altun, A. & Thiel, W. Theoretical perspective on the structure and mechanism of cytochrome P450 enzymes. *Chem. Rev.* **105,** 2279–2328 (2005).
41. Ortiz de Montellano, P. R. & De Voss, J. J. Oxidizing species in the mechanism of cytochrome P450. *Nat. Prod. Rep.* **19,** 477–493 (2002).
42. Shaik, S., Lai, W., Chen, H., Wang, Y. The valence bond way: reactivity patterns of cytochrome P450 enzymes and synthetic analogs. *Acc. Chem. Res.* **43,** 1154–1165 (2010).
43. Shaik, S., Milko, P., Schyman, P., Usharani, D. & Chen, H. Trends in aromatic oxidation reactions catalyzed by cytochrome P450 enzymes: a valence bond modeling. *J. Chem. Theory Comput.* **7,** 327–339 (2011).
44. Bukowski, M. R. *et al.* A thiolate-ligated nonheme oxoiron(IV) complex relevant to cytochrome P450. *Science* **310,** 1000–1002 (2005).
45. Cho, K.-B., Hirao, H., Shaik, S. & Nam, W. To rebound or dissociate? This is the mechanistic question in C–H hydroxylation by heme and nonheme metal-oxo complexes. *Chem. Soc. Rev.* **46,** 1197–1210 (2016).
46. Shaik, S., Chen, H. & Janardanan, D. Exchange-enhanced reactivity in bond activation by metal-oxo enzymes and synthetic reagents. *Nat. Chem.* **3,** 19–27 (2011).

47. Arabi, A. A. & Matta, C. F. Effects of external electric fields on double proton transfer kinetics in the formic acid dimer. *Phys. Chem. Chem. Phys.* **13,** 13738–13748 (2011).
48. Ceron-Carrasco, J. P., Cerezo, J. & Jacquemin, D. How DNA is damaged by external electric fields: selective mutation vs. random degradation. *Phys. Chem. Chem. Phys.* **16,** 8243–8246 (2014).
49. Carbonell, E., Duran, M., Lledos, A. & Bertran, J. Catalysis of Friedel–Crafts reactions by electric fields. *J. Phys. Chem.* **95,** 179–183 (1991).
50. Zhou, Z. J. *et al.* Electric field-driven acid-base chemistry: proton transfer from acid (HCl) to base (NH_3/H_2O). *J. Phys. Chem. A* **115,** 1418–1422 (2011).
51. Oklejas, V., Uibel, R. H., Horton, R. & Harris, J. M. Electric-field control of the tautomerization and metal ion binding reactivity of 8-hydroxyquinoline immobilized to an electrode surface. *Anal. Chem.* **80,** 1891–1901 (2008).
52. Timerghazin, Q. K. & Talipov, M. R. Unprecedented external electric field effects on S-nitrosothiols: possible mechanism of biological regulation? *J. Phys. Chem. Lett.* **4,** 1034–1038 (2013).
53. De Biase, P. M., Doctorovich, F., Murgida, D. H. & Estrin, D. A. Electric field effects on the reactivity of heme model systems. *Chem. Phys. Lett.* **434,** 121–126 (2007).
54. Saita, A. M. & Saija, F. Miller experiments in atomistic computer simulation. *Proc. Natl. Acad. Sci. USA* **111,** 13768–13773 (2014).
55. Jissy, A. K. & Datta, A. Effect of external electric field on H-bonding and π-stacking in guanine aggregates. *ChemPhysChem* **13,** 4163–4172 (2012).
56. Woodward, R. B. & Hoffmann, R. *The conservation of orbital symmetry* (Chemie, GmbH 1970).
57. Gryn'ova, G. & Coote, M. L. Origin and scope of long-range stabilizing interactions and associated SOMO–HOMO conversion in distonic radical anions. *J. Am. Chem. Soc.* **135,** 15392–15403 (2013).
58. Gooding, J. J. & Ciampi, S. The molecular level modification of surfaces: from self-assembled monolayers to complex molecular assemblies. *Chem. Soc. Rev.* **40,** 2704–2718 (2011).
59. Zhang, L. *et al.* TEMPO monolayers on Si(100) electrodes: electrostatic effects by the electrolyte and semiconduuctor space-charge on the electroactivity of a persistent radical. *J. Am.Chem. Soc.* **138,** 9611–9619 (2016).

Additional information

Supplementary information is available in the online version of the paper. Reprints and permissions information is available online at www.nature.com/reprints. Correspondence and requests for materials should be addressed to S.S.

Competing financial interests

The authors declare no competing financial interests.